Discovery of a High Affinity Adenosine A₁/A₃ Receptor Antagonist with a Novel 7-Amino-pyrazolo[3,4-d]pyridazine Scaffold

Anna Suchankova,[†] Margarita Stampelou,[†] Klontiana Koutsouki,[†] Athanasios Pousias, Lakshiv Dhingra, Kerry Barkan, Nicole Pouli, Panagiotis Marakos, Roxane Tenta, Antonios Kolocouris,* Nikolaos Lougiakis,* and Graham Ladds*

ACCESS | Metrics & More | Article Recommendations | SI Supporting Information

ABSTRACT: Here we describe the design and synthesis of pyrazolo[3,4-d]pyridazines as adenosine receptor (AR) ligands. We demonstrate that the introduction of a 3-phenyl group, together with a 7-benzylamino and 1-methyl group at the pyrazolopyridazine scaffold, generated the antagonist compound **10b**, which displayed 21 nM affinity and a residence time of ∼60 min, for the human A₁R, 55 nM affinity and a residence time of ∼73 min, for the human A₃R and 1.7 μM affinity for the human A₂BR while not being toxic. Strikingly, the 2-methyl analog of **10b**, **15b**, had no significant affinity. Docking calculations and molecular dynamics simulations of the ligands inside the orthosteric binding area suggested that the 2-methyl group in **15b** hinders the formation of hydrogen bonding interactions with $N^{6.55}$ which are considered critical for the stabilization inside the orthosteric binding cavity. We, therefore, demonstrate that **10a** is a novel scaffold for the development of high affinity AR ligands. From the mutagenesis experiments the biggest effect was observed for the Y271$^{7.46}$A mutation which caused an ∼10-fold reduction in the binding affinity of **10b**.

KEYWORDS: Adenosine A₁ receptor, adenosine A₃ receptor, adenosine A₂B receptor, antagonist, binding kinetics, BRET, cAMP, cytotoxicity, molecular dynamics, mutagenesis, residence time
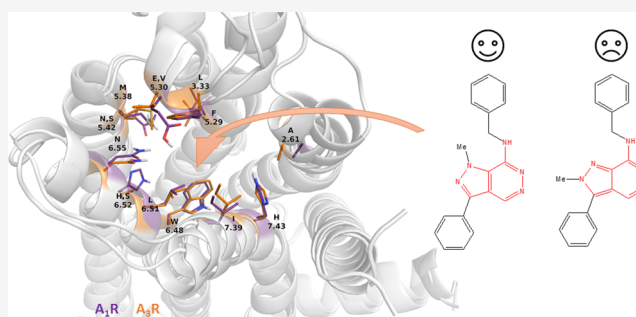
Adenosine, a naturally occurring purine nucleoside, is the endogenous agonist of adenosine receptors (ARs).[1] ARs are G protein-coupled receptors (GPCRs) comprising four subtypes; A₁, A₂A, A₂B, and A₃. The A₂A and A₂B subtypes act synergistically with Gα_s stimulating adenylyl cyclase and, therefore, increasing 3′,5′-cyclic adenosine monophosphate (cAMP) levels. In contrast, A₁ and A₃ receptor subtypes inhibit adenylyl cyclase and decrease cAMP levels by coupling to the G$_{i/o}$ family of G proteins.

In the last two decades numerous heterocyclic compounds have been synthesized as AR ligands including xanthines and bi- or tricyclic fused heterocyclic analogues, e.g., purines, deazapurines, pyrazolopyridines, imidazotriazines, thienopyridazines, naphthyridines, pyridopyrimidines, and pyrazoloquinolines.[2−4]

Different therapeutic applications have been identified in preclinical and clinical studies for A₁R antagonists as potassium-sparing diuretic agents with kidney-protecting properties,[2] treatments for chronic lung diseases such as asthma,[5,6] and possible use in Parkinson's disease.[7]

A₃R has been reported to be overexpressed in several types of cancer cells and is, thus, considered as a biological marker for tumors.[8] In a recent study, the potent and selective A₃R antagonist LJ-1888 ((2R,3R,4S)-2-[2-chloro-6-(3-iodobenzylamino)-9H-purin-9-yl]tetrahydrothiophene-3,4-diol) blocked the development and attenuated the progression of renal interstitial fibrosis,[9] while A₃R antagonists have demonstrated efficacy in eye pathologies by lowering intraocular pressure.[10]

While the binding mode of several agonists and antagonists at A₁R has been revealed with X-ray crystallography or cryogenic electron microscopy,[11−13] the experimental structures for A₃R and A₂BR have, to date, not been resolved, and only homology models can be used for these AR subtypes.

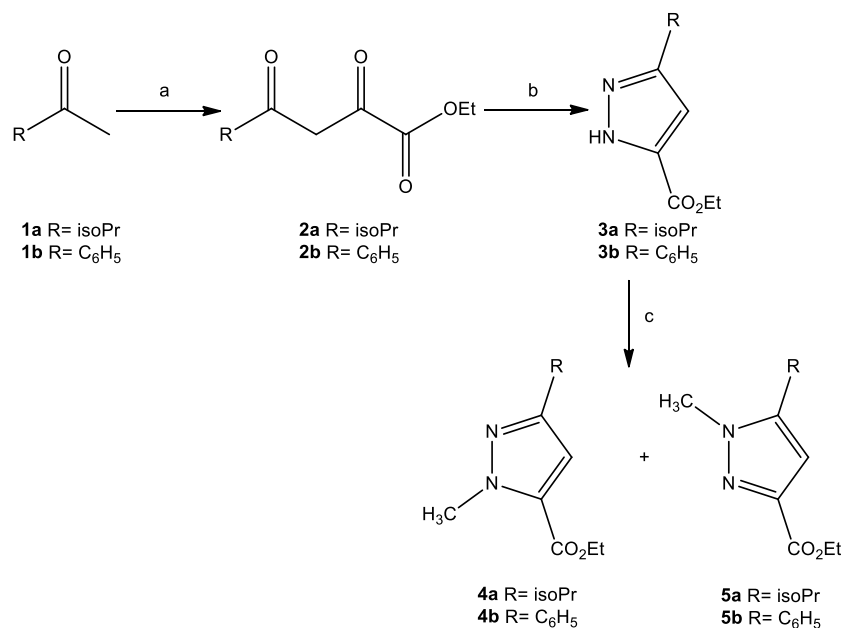By the repurposing of antiproliferative aromatic condensed nitrogen heterocycles, we previously identified nanomolar affinity pyrazolo[3,4-c]pyridine A₁R/A₃R antagonists.[14] It has been reported that non-xanthine pyrazolo derivatives that potently bind ARs are pyrazolo[4,3-d]pyrimidines,[3] pyrazolo-
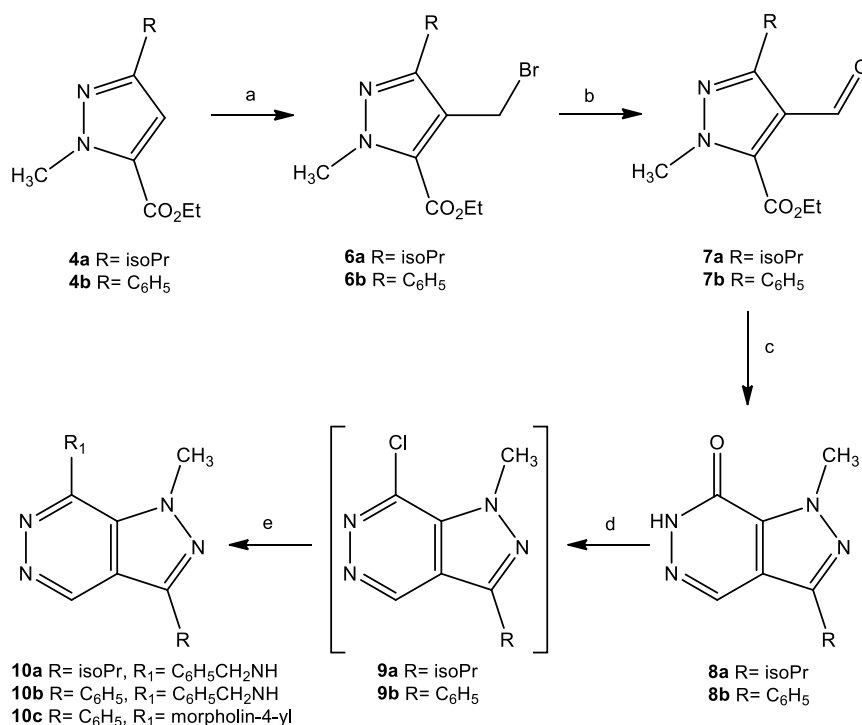
Scheme 1. Synthesis of 4a,b and 5a,b[a]

1a R= isoPr
1b R= C₆H₅

2a R= isoPr
2b R= C₆H₅

3a R= isoPr
3b R= C₆H₅

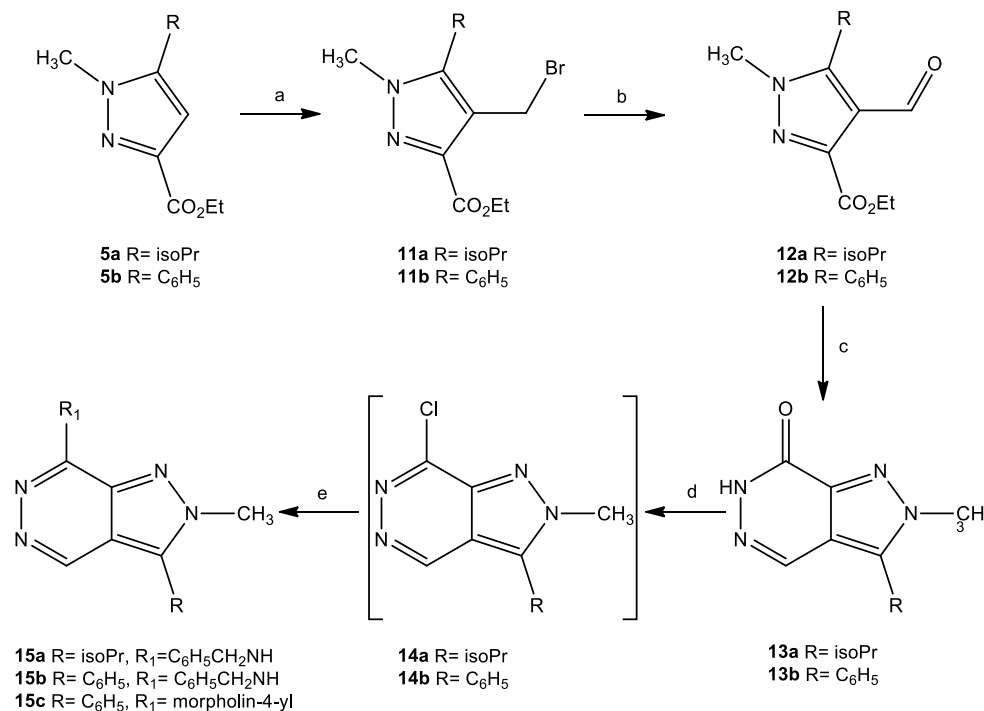**4a** R= isoPr
4b R= C₆H₅

5a R= isoPr
5b R= C₆H₅

[a]Reagents and conditions: (a) diethyl oxalate, NaH 60%, toluene dry, 50°C, 2 h; (b) NH₂NH₂ 80%, EtOH, reflux, 90 min; (c) (i) NaH 60%, DMF dry, 0 °C, 15 min, (ii) CH₃I, rt, 1 h.

Scheme 2. Synthesis of 10a−c[a]

4a R= isoPr
4b R= C₆H₅

6a R= isoPr
6b R= C₆H₅

7a R= isoPr
7b R= C₆H₅

8a R= isoPr
8b R= C₆H₅

9a R= isoPr
9b R= C₆H₅

10a R= isoPr, R₁= C₆H₅CH₂NH
10b R= C₆H₅, R₁= C₆H₅CH₂NH
10c R= C₆H₅, R₁= morpholin-4-yl

[a]Reagents and conditions: (a) paraformaldehyde, 33% HBr in AcOH, 90 °C, 3.5 h; (b) N-methylmorpholine-N-oxide, MeCN dry, rt, 24 h; (c) NH₂NH₂ (80%), HCl 36%, EtOH, 90°C, 1 h; (d) POCl₃, 110 °C, 2.5−8 h; (e) HNR₁R₂, EtOH, reflux, 2 h.

[1,5-c]quinazolines,[15] pyrazolo[3,4-b]pyridines,[16,17] pyrazolo-[3,4-b]pyridines, pyrazolo[4,3-e]-1,2,4-triazolo[1,5-c]-pyrimidines, pyrazolo[3,4-c]- or -[4,3-c]quinolines, pyrazolo-[4,3-d]pyrimidinones, pyrazolo[3,4-d]pyrimidines, and pyrazolo[1,5-a]pyridines.[18] After we previously identified the potent pyrazolo[3,4-c]pyridine A₁R/A₃R antagonists[14] and observed that certain substituted pyrazolo[3,4-b]pyridines had

antagonistic potency against A₃R or A₁R,[16,17] we quantified the novel pyrazolo[3,4-d]pyridazine scaffold for activity at ARs. Here, we synthesized a series of new 3-alkyl- or 3-aryl-7-amino-pyrazolo-[3,4-d]pyridazine derivatives and determined their affinities against the different ARs using functional cAMP accumulation assays, fluorescent ligand displacement binding studies, and molecular dynamics (MD) simulations.[19,20] We

Scheme 3. Synthesis of 15a−c[a]

5a R= isoPr
5b R= C6H5

11a R= isoPr
11b R= C6H5

12a R= isoPr
12b R= C6H5

15a R= isoPr, R1=C6H5CH2NH
15b R= C6H5, R1= C6H5CH2NH
15c R= C6H5, R1= morpholin-4-yl

14a R= isoPr
14b R= C6H5

13a R= isoPr
13b R= C6H5

[a]Reagents and conditions: (a) paraformaldehyde, 33% HBr in AcOH, 90 °C, 3.5 h; (b) N-methylmorpholine-N-oxide, MeCN dry, rt, 24 h; (c) NH2NH2 (80%), HCl 36%, EtOH, 90 °C, 1 h; (d) POCl3, 110 °C, 2.5−8 h; (e) HNR1R2, EtOH, reflux, 2 h.

identified the 21 nM A_1R/55 nM A_3R/<2 μM $A_{2B}R$ antagonist 1-methyl-3-phenyl-7-benzylaminopyrazolo[3,4-d]pyridazine (10b) as a lead compound. Strikingly, compound 15b, the 2-methyl congener of 10b, had lower affinity by >100-fold against 3AR subtypes since, we assumed, it cannot form hydrogen bonding interactions with $N^{6.55}$ which are considered critical for stabilization inside the orthosteric binding cavity. Finally, as these new compounds present structural similarity to antiproliferative purine analogues,[21] we evaluated their cytotoxic potential against the human fibroblasts cell line (WI-38) and prostatic (PC-3) and colonic (HCT116) cancer cell lines.

Similarity Calculations. Searching the CHEMBL[22] database to determine if pyrazolo[3,4-d]pyridazine has been used as a scaffold for ligands binding to ARs, using a TanimotoCombo (Tc)[23] coefficient > 0.85, we did not find any pyrazolo[3,4-d]pyridazine derivatives with potency against ARs, suggesting that it is a novel ring system for the development of AR ligands. When we considered the amide 7-benzylamino-3-phenylpyrazolo[3,4-d]pyridazine, we found the 4-(2-phenethyl)amino 1-phenylethylpyrazolo[3,4-b]pyridine (Tc = 0.15) had been reported to bind A_1R.[16,17] Thus, we proceeded with a structural activity relationship study around 7-benzylamino-3-phenyl pyrazolo[3,4-d]pyridazine and synthesized a series of 7-amino-pyrazolo[3,4-d]pyridazines for biological evaluation against ARs.

Chemistry. The synthesis of the target compounds was accomplished through the previously reported pyrazolecarboxylates 4a,b and 5a,b (Scheme 1). Briefly, commercial isopropylmethylketone (1a) or acetophenone (1b), was first converted to the ethyl 2,4-diketocarboxylates 2a and 2b, respectively,[24,25] which upon reaction with hydrazine monohydrate gave the pyrazolecarboxylates 3a,b.[26] These were methylated using methyl iodide in the presence of sodium hydride and provided the regioisomers 4a,b[27,28] and 5a,b,[28]

respectively. Interestingly, when we used tetrahydrofuran as solvent in the place of dimethylformamide (DMF), we exclusively obtained the N^1-methyl-5-carboxylate 4a isomer.

Each of the isomeric pyrazoles 4a,b or 5a,b was subsequently treated with paraformaldehyde in the presence of a 33% HBr solution in acetic acid and was converted to the bromides 6a,b (Scheme 2) or 11a,b (Scheme 3), respectively. The bromomethyl group was then oxidized using N-methylmorpholine N-oxide to generate the carbaldehydes 7a,b (Scheme 2) and 12a,b (Scheme 3).

The aldehydes 7a,b and 12a,b were then treated with hydrazine, and upon ring closure the pyrazolopyridazinones 8a,b and 13a,b were obtained. The pyridazinones reacted with phosphorus oxychloride to give the corresponding chloro derivatives 9a,b and 14a,b with suitable purity that they could be introduced to the next reaction. These crude products were then treated with benzylamine or morpholine to result in the target compounds 10a−c and 15a−c (Figures S1−S3).

Assessing Biological Activity of Pyrazolo[3,4-d]-pyridazine Derivatives. *cAMP Assays Assessing Activity at Adenosine Receptors.* Having synthesized compounds 10a−c and 15a−c, we next tested their activity, as antagonists, against the different human AR subtypes using a single high concentration of the compound (1 μM) coadministered with NECA (5′-N-ethylcarboxamidoadenosine) in a cAMP accumulation assay (Figure 1A and B). Note that for A_1R and A_3R 10 μM forskolin was added since these are $G_{i/o}$-coupled receptors and reduce cAMP accumulation.[19,29] All compounds lacked efficacy at NECA-stimulated $A_{2A}R$ (even when tested at 10 μM) (Table S1). Compounds 10c, 15b, and 15c also lacked efficacy at the other 3AR subtypes, with 15a displaying weak efficacy only at A_3R, while compounds 10a and 10b displayed activity at all 3ARs although this was only detectable for $A_{2B}R$ when a 10 μM concentration of the compound was used (Table S1). Based
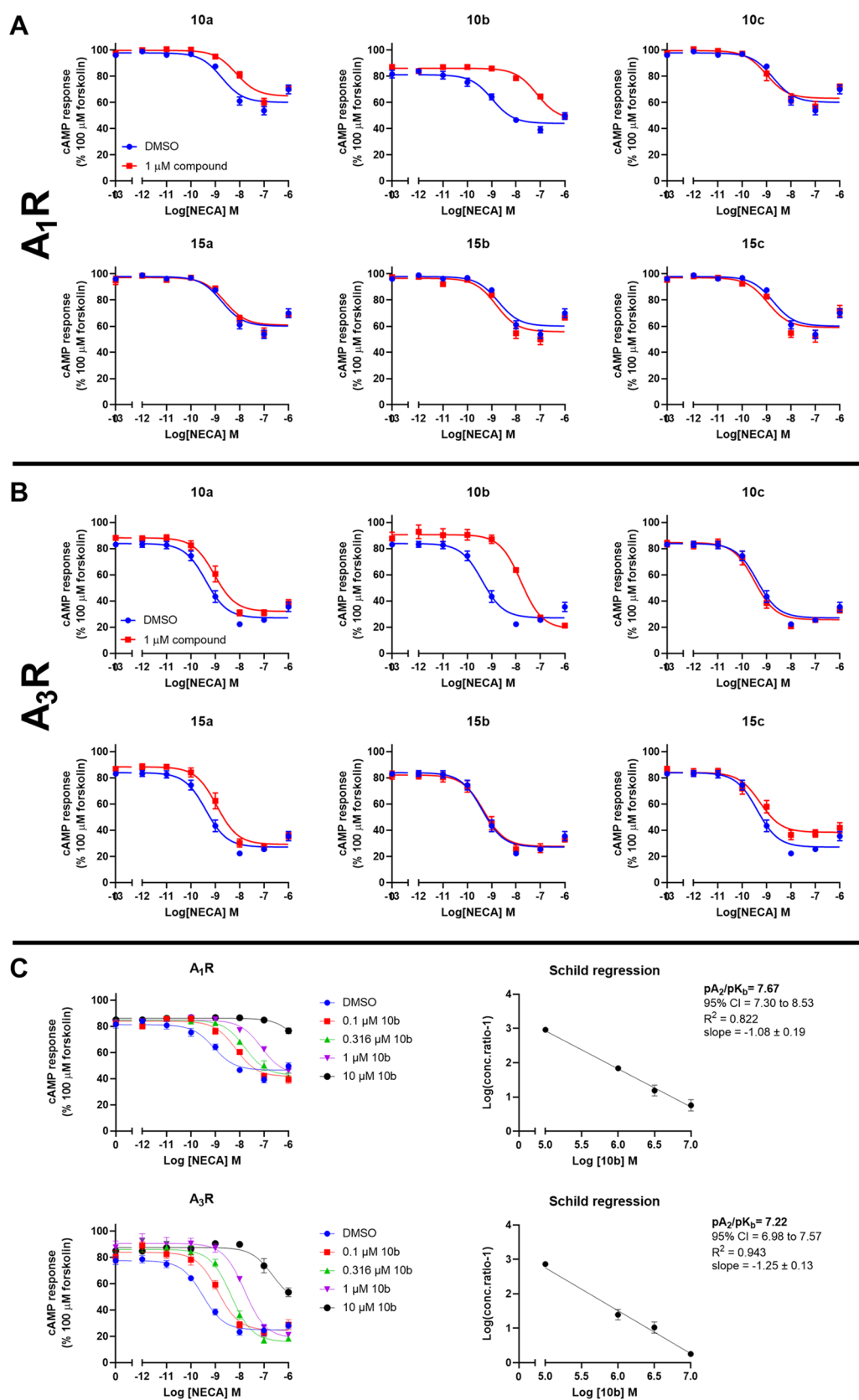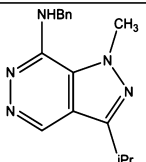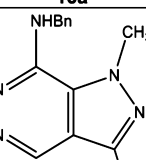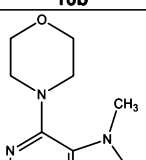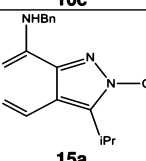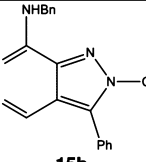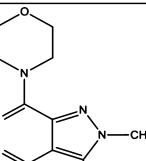
Figure 1. Characterization of 7-amino-pyrazolo[3,4-d]pyridazines at human A_1R and A_3R. (A and B) Cells expressing either human A_1R (A) or A_3R (B) were exposed to 10 μM forskolin and stimulated with increasing concentrations of NECA for 30 min in the presence of a 1 μM concentration of the test compound, and the cAMP accumulation was quantified. (C) cAMP accumulation was measured as detailed in part A using multiple concentrations of **10b**. Using pEC$_{50}$ values, Schild regression analysis was conducted to calculate pA$_2$/pK_b values. All values are mean ± SEM expressed as percentage forskolin inhibition, relative to NECA. $n \geq 3$ independent experimental repeats were performed in duplicate.

Table 1. Chemical Structures, Antagonistic Potencies (pEC$_{50}$ in the Presence of NECA^{a}), and Affinities (pK$_i$^{b}) of 7-Amino-pyrazolo[3,4-d]pyridazines 10a−c and 15a−c against A$_1$R and A$_3$R

Compound	A$_1$R		A$_3$R	
	pEC$_{50}$ of NECA in presence of compound^a	pK$_i$^{b}	pEC$_{50}$ of NECA in presence of compound^a	pK$_i$^{b}
10a	8.15 ± 0.12**	5.17 ± 1.13#	9.04 ± 0.11	6.42 ± 0.28
10b	7.15 ± 0.07***	7.95 ± 0.09***	7.80 ± 0.10***	7.89 ± 0.11*
10c	9.01 ± 0.16	< 5.0	9.50 ± 0.12	< 5.0
15a	8.62 ± 0.15	<5.0	8.94 ± 0.11*	5.77 ± 0.27#
15b	8.82 ± 0.15	< 5.0	9.33 ± 0.13	< 5.0
15c	8.96 ± 0.18	< 5.0	9.27 ± 0.16	6.44 ± 0.23#
DPCPX	6.03 ± 0.16	9.23 ± 0.08	-	-
MRS1220	7.32 ± 0.09	7.29 ± 0.27	7.44 ± 0.02#	9.94 ±0.11
NECA	8.74 ± 0.15	6.69 ± 0.10	9.39 ± 0.11	7.05 ± 0.07

^{a}Mean ± SEM; functional activities (pEC$_{50}$ values of NECA in the presence of either 1 μM ligands or vehicle) as mean ± standard error of the mean (SEM) of at least three independent repeats, conducted in duplicate—values obtained from Figure 1. ^{b}Mean ± SEM; equilibrium binding affinities of the ligands measured with NanoBRET against Nluc-A$_3$R or Nluc-A$_1$R; NECA was used as positive control.[3] $^\#$Due to the high affinity of MRS1220, 10 nM was used to enable measurement of the full dose−response curve of NECA to determine pEC$_{50}$. Statistical significance compared to NECA was determined, at $p < 0.05$, through one-way ANOVA with Dunnett's post-test (*, $p < 0.05$; **, $p < 0.01$; ***, $p < 0.001$; ****, $p < 0.0001$).

upon a single concentration of antagonist, we calculated the equilibrium dissociation constant (pK$_d$) of each compound (Table 1). Of the compounds tested, **10b** displayed the highest affinity at the different AR subtypes with greater selectivity toward A$_1$R and A$_3$R than A$_{2B}$R. We next performed a more

extensive Schild analysis using multiple doses of the most potent antagonist, **10b**, only at A$_1$R and A$_3$R (Figure 1C). In both cases **10b** acted as a competitive antagonist, generating a Schild slope that did not significantly differ from unity. Using the Schild plot,
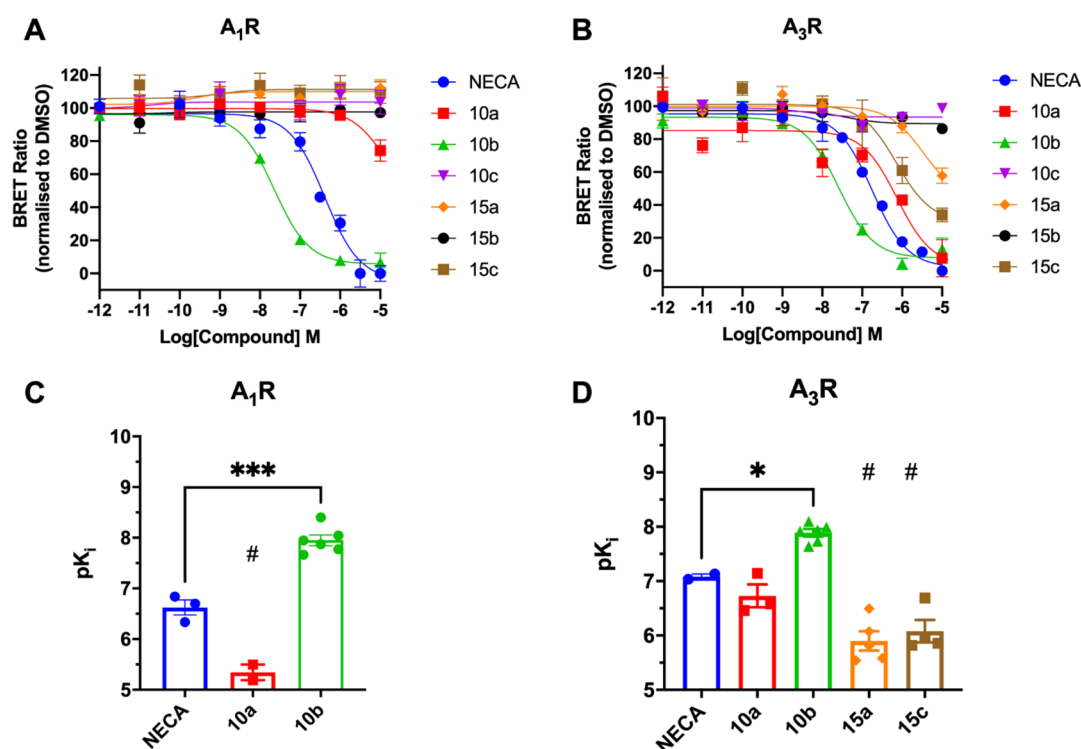
Figure 2. Inhibition of BRET between CA200645 at NLuc-A_1R and Nluc-A_3R by **10b** and **10a**. HEK293 cells expressing Nluc-A_1R (A) or Nluc-A_3R (B) were treated with 5 nM or 20 nM CA200645, respectively, enabling concentration-dependent decreases in the BRET ratio at 10 min to be determined with the response normalized to DMSO. Binding curves were fitted with the Cheng Prusoff equation built into GraphPad Prism 9.3 to enable estimates of the pK_i.[19] Comparison of pK_i values for A_1R (C) and A_3R (D) as determined via BRET binding. Each data point represents the mean ± SEM of at least three experiments performed in duplicate. The statistical significance compared to NECA was determined, at $p < 0.05$, through one-way ANOVA with Dunnett's post-test (*, $p < 0.05$; ***, $p < 0.001$). #Compounds did not fully displace CA200645, so pK_i values are estimates preventing statistical analysis.

we calculated **10b**'s affinity (pA_2/pK_b) to be 21 nM at A_1R and 55 nM at A_3R while only 1.7 μM at A_{2B}R (Table S1).

Quantifying Binding Parameters Using a NanoBRET-Based Saturation Binding Assay. We next sought to independently verify the affinities determined using the Shield analysis by directly quantifying the potential antagonists' binding to A_1R and A_3R using a previously described saturation nano-bioluminescence resonance energy transfer (NanoBRET) binding assay.[19] We determined the ability of all the compounds to displace the specific binding of CA200645,[30] a fluorescent antagonist of A_3R and A_1R, using Nluc-A_3R expressing human embryonic kidney 293 (HEK293) and Nluc-A_1R HEK293 cells (Figure 2 and Table 1). A_{2B}R was not included in this analysis since the pK_d values of **10a** and **10b** at A_{2B}R were estimated to be below 1 μM (Figure 1 and Table 1). Consistent with the Schild analysis, compound **10b** displayed the highest affinity at A_1R and A_3R (A_1R, pK_i = 7.95 ± 0.09; A_3R, pK_i = 7.89 ± 0.11). Of the remaining compounds, **10a** displayed weak affinity at A_3R (pK_i, 6.42 ± 0.28), which agreed with the Schild regression estimate, but failed to fully displace CA200645 at A_1R, making an estimate for its affinity unreliable. All the other compounds failed to displace CA200645 at A_1R or A_3R except for **15a** and **15c**, which did display some binding at A_3R but, like **10a**, also failed to fully displace CA200645 at the concentrations tested. Significantly, **15b**, which contains an *N*-methyl substitution to 1-NH and 2-NMe compared to 1-NMe and 2-NH in **10b**, failed to bind either AR subtype.

Determining Kinetic Parameters of 10b Binding at A_3R and A_1R Using NanoBRET. We next investigated the real-time

binding kinetics[19,30] of **10b** at A_3R and A_1R using the NanoBRET binding method. Specifically, we quantified **10b**'s ability to inhibit specific binding of CA200645 to Nluc-A_3R and Nluc-A_1R expressed in HEK293 cells. The kinetic parameters for CA200645 binding at Nluc-A_3R were previously determined as K_{on} = 32.5 ± 0.28 × 10^5 M^{-1} min^{-1} and K_{off} = 0.025 ± 0.005 min^{-1} with a pK_D of 10.11. Conversely the kinetics of CA200645 binding at Nluc-A_1R were determined as K_{on} = 14.5 ± 0.4 × 10^5 M^{-1} min^{-1}, K_{off} = 0.023 ± 0.001 min^{-1}, and pK_D = 7.80 ± 0.2 nM.[14] Applying these parameters into the "kinetics of competitive binding" model built into GraphPad Prism9.0, we were able to provide estimates of the kinetics of binding for **10b** against A_1R (K_{on} = 51.4 ± 0.26 × 10^5 M^{-1} min^{-1}, K_{off} = 0.019 ± 0.003 min^{-1} with a pK_D = 7.46 ± 0.1 and RT = 59.8 ± 12.7 min) and against the A_3R, (K_{on} = 25.6 ± 0.1 × 10^5 M^{-1}min^{-1}, K_{off} = 0.0014 ± 0.002 min^{-1} with a pK_D = 7.26 ± 0.05 and RT = 72.58 ± 8.8 min). None of the other compounds were analyzed using this method due to their extremely fast K_{off} rates (>min^{-1}). For compound **10b** there was an excellent agreement between pK_D (K_{on}/K_{off}) of the compounds from the kinetics assays and the Schild analysis (pA_2/pK_b) and fair agreement (~3.16-fold) with the saturation binding assays (pK_i).

Simulations. *Investigation of the Binding of the 7-Amino-pyrazolo[3,4-d]pyridazines to A_1R and A_3R.* Having pharmacologically evaluated the different compounds, we then used molecular docking to provide insights into how they bind to the ARs. We docked **10a**−**10c** into the orthosteric binding site of A_1R and **10b** and **15b** into A_{2B}R and A_3R (the amino acid sequences of A_1R, A_3R, and A_{2B}R in the orthosteric binding area

Figure 3. continued

Figure 3. (A−C) 100 ns MD simulations of **10a−c** inside the orthosteric binding area of A_1R. (D) 100 ns MD simulations of **15b** inside the orthosteric binding area of A_1R. Starting structures are shown (docking pose), and representative frames from MD simulations, receptor−ligand interaction frequency histograms, and RMSD plots of proteins ($RMSD_{protein}$; blue plots) and ligand heavy atoms ($RMSD_{ligand}$; red plots) inside the orthosteric binding area of WT A_1R or A_3R. Bars are plotted only for residues with interaction frequencies ≥0.2. Color scheme: ligand = brown sticks, receptor = white cartoon and sticks, hydrogen bonding interactions = yellow (dashes or bars), $\pi-\pi$ interactions = green (dashes or bars), hydrophobic interactions = gray, water bridges = blue. For the protein models of A_1R in complex with **10a−c** or **15b**, the experimental structure of the inactive form of A_1R in complex with an antagonist (PDB ID 5UEN[4]) was used.
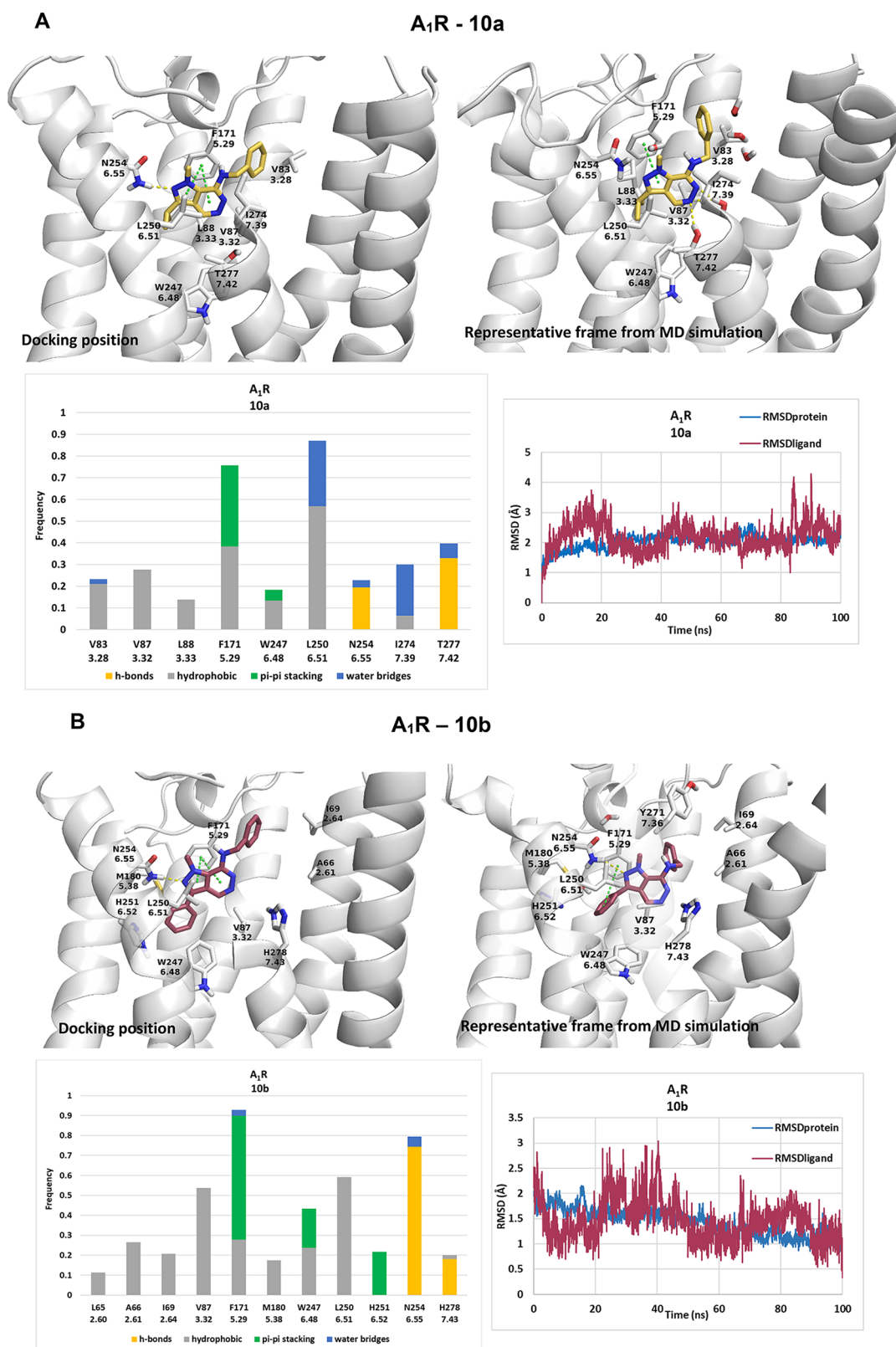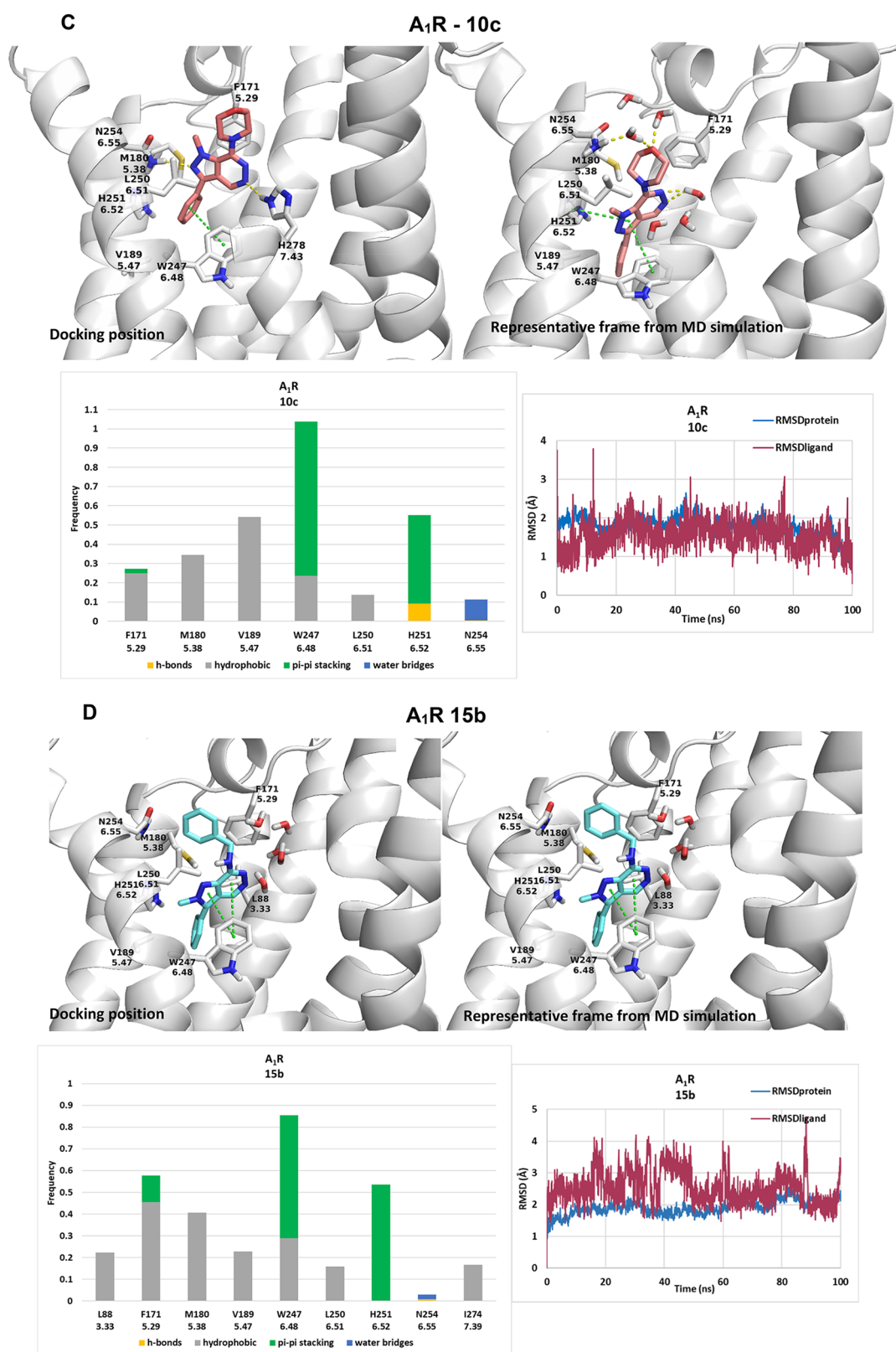
are shown in Scheme S1) using ChemScore as the scoring function[31] with the highest score docking pose being inserted into a hydrated phosphatidylethanolamine bilayer. The complexes were subjected to 100 ns MD simulations with amber99sb,[32] and then, the MD simulations' trajectory was analyzed (Table S2). The MD simulations showed that the 7-benzylamino-pyrazolo[3,4-d]pyridazine **10b** substituted with N^1Me and a 3-phenyl group formed a stable complex with all 3ARs with $RMSD_{protein}$ values <2.1 Å. Starting from the same docking pose of **10b** in A_1R or A_3R (Figure 3), the mean frame from MD simulations was close to the starting docking pose in A_1R ($RMSD_{lig}$ = 1.21 Å) while in A_3R (Figure S2) the ligand moved considerably into the cleft between the transmembrane (TM)3, TM5, and TM6 helices ($RMSD_{lig}$ = 4.88 Å). Thus, starting from the same binding pose for **10b**, the MD simulations produced two different binding orientations at A_1R and A_3R. This is due to the fact that A_1R has a broader binding area, expanded toward TM1 and TM2, compared to the other ARs, according to the X-ray structures of A_1R in complex with antagonists.[11,12] A similar AR ligand reported in the literature is 4-(2-phenethyl)amino 1-phenylethyl pyrazolo[3,4-b]pyridine (Tc = 0.15), which binds with a similar docking pose to **10b** to A_1R.[16] We also docked a representative adenine derivative (N9-methyl,N6-benzyl adenine) to A_1R and found a similar docking pose (Figure S3).

Inside the A_1R orthosteric site, compound **10b** formed hydrogen bonds through its pyrazole or pyridazine nitrogen donor groups to the amide side chain of $N254^{6.5}$ or the imidazole side chain of $H278^{7.43}$. Furthermore, **10b** was stabilized in the orthosteric binding site through $\pi-\pi$ interactions between its pyrazolo[3,4-d]pyridazine or phenyl rings with $F171^{5.29}$, $H251^{6.2}$, and $W247^{6.48}$, respectively. The benzylamino group of **10b** oriented toward the widened TM2 area in A_1R, forming hydrophobic interactions with $A66^{2.61}$ and $I69^{2.64}$. Furthermore, **10b** was found to bind deep in the pocket interacting with $V87^{3.32}$ and $W247^{6.48}$ while 3-phenyl-pyrazole aligned close to the side chains of $M180^{5.38}$ and $L250^{6.1}$ (Figure 3A). In A_3R, compound **10b** was stabilized through formation of hydrogen bonding interactions with $N254^{6.5}$ and $H278^{7.43}$ and hydrophobic interactions with $L90^{3.32}$, $L91^{3.33}$, $F168^{5.29}$, $M177^{5.38}$, $L246^{6.1}$, and $I268^{7.39}$ (Figure S2B). Finally, the MD simulations for **10b** (Figure S2A) in complex with $A_{2B}R$ (Figure S2) show weak hydrogen bond interactions with $N254^{6.5}$.

Pharmacologically, compounds **10b** and **15b** differed considerably in their affinity to the ARs (Figures 1 and 2 and Table 1). Comparing MD simulations for **15b** with **10b** in the orthosteric binding area of A_1R, A_3R (and $A_{2B}R$) shows that starting from a similar docking pose, the substitution from N^1Me and 2-NH (found in **10b**) to N^1H and N^2Me (in **15b**) results in **15b** failing to generate hydrogen bonds with $N^{6.55}$ because of the steric repulsion between 2-methyl and the amide side chain of $N^{6.55}$; for this reason also **15a** and **15c** were inactive (Figure S2). Although many ligands can have similar docking poses, subtle changes in the ligand substitution pattern can result in significant changes in binding, and this can be followed only with MD simulations. Considering the two active compounds, **10b** and **10a**, replacement of the 3-phenyl group (found in **10b**) with a 3-isopropyl group (generating **10a**) results in a remarkable reduction of affinity. This is due to **10a** losing significant $\pi-\pi$ interactions with $H251^{6.2}$ and hydrophobic interactions with residues deeper in the binding site, e.g., $W247^{6.48}$, $L250^{6.1}$, and $V87^{3.32}$ (Figure 3). Finally, substitution of **10b**'s 7-benzylamino by the more rigid morpholinyl group

(found in **10c**) resulted in reduced affinity to the ARs. The more rigid morpholino group in **10c** repels $F171^{5.29}$, so the ligand rotates and moves to the bottom of the binding area, losing hydrogen bonding interactions with $N254^{6.5}$ and weakening its hydrophobic interaction with critical residues, e.g., $F171^{5.29}$ and $L250^{6.1}$ (Figure 3). With an accuracy of $\sim\pm4$ kcal mol^{-1}, the MM-GBSA method[33,34] (Supporting Information) only provides an approximation when applied to structure–activity relationships for analogs in the same series. Nevertheless, the MM-GBSA binding free energy calculations for ligands **10a–c** against A_1R (Table S2), using the OPLS2005 force field[35,36] with a hydrophobic slab as an implicit membrane model and including the waters in the orthosteric binding area, predicted fairly well the stability of **10a–c** in complex with A_1R with binding free energy values (after neglecting entropy) ΔG_{eff} = −94.50, −96.42, and −85.35 kcal mol^{-1}.

Mutagenesis Experiments to Study 10b Binding to A_1R. We have previously observed that mutation of residues that do not directly interact with the ligands (e.g., $V^{5.30}$ for A_3R, which is more than 4 Å apart from the ligand inside the orthosteric binding area) can, through allosteric interactions due to the plasticity of the binding area, significantly affect ligand affinity.[20,21,37] As such it is not always straightforward to determine the effects of a mutation on affinity properties. Despite this caveat, we next used mutational analysis combined with NanoBRET to determine the important residues required for **10b** binding to A_1R. The mutation of $L250^{6.1}$A resulted in only a slight reduction of binding affinity for **10b** (Table 2)

Table 2. Binding Affinities (pK_i) for 10b Measured Using Saturation NanoBRET Binding with CA200645 as the Fluorescent Tracer against WT A_1R and Mutant A_1Rs

A_1R	pK_i	Effect on affinity
WT	7.68 ± 0.11	baseline
$T91^{3.36}$A	7.68 ± 0.07	no change
$E172^{5.30}$A	7.34 ± 0.06	no significant change
$L250^{6.51}$A	7.57 ± 0.04	no significant change
$H251^{6.52}$A	7.62 ± 0.06	no significant change
$S267^{7.42}$A	7.86 ± 0.03	no significant change
$Y271^{7.46}$A	6.99 ± 0.05	$\sim$10-fold reduction

despite the MD simulations suggesting that the ligand should be close enough to $L250^{6.1}$ to enable hydrophobic interactions. It is possible that residues $H251^{6.52}$ and $W247^{6.48}$ could contribute to the stabilization of **10b** with hydrophobic interactions even if $L250^{6.1}$ is mutated to alanine. It is noteworthy that mutation of $E172^{5.30}$ (which is also more than 4 Å apart from the ligand inside the orthosteric binding area) to alanine also did not significantly change the binding affinity (Table 2). This contrasts with our studies using 3-phenyl-7-anilinopyrazolo-[3,4-c]pyridines which showed a 1.5-fold decrease in affinity due to the $E172^{5.30}$A mutation.[14]

In addition, mutation of $H251^{6.2}$A has been reported to reduce antagonist affinity against A_3R[20,21] although here it did not have any effect on **10b** affinity at A_1R. Other residues of interest to mutate were $T91^{3.36}$A and $S267^{7.42}$A, which are deep in the orthosteric pocket. Interestingly, we found that mutation to alanine of these residues also did not have a significant effect on the binding affinity of **10b** (Table 2). This is in contrast to our results for pyrazolo[3,4-c]pyridines which can interact directly with these residues.[9] The results for **10b** suggested that it is

positioned above pyrazolo[3,4-c]pyridines,[9] in the A_1R pocket, and so unaffected by these mutations.

The biggest effect in this study was observed for the $Y271^{7.46}A$ A_1R mutation, which caused a ~10-fold reduction in the binding affinity of **10b** (Table 2). This effect is in contrast to that observed previously for pyrazolo[3,4-c]pyridines[14] for which we showed that the $Y271^{7.46}A$ mutation caused a slight increase in binding affinity. Since the MD simulations showed contacts with $H278^{7.43}$ and not $Y271^{7.46}$, the $Y271^{7.46}A$ mutation in A_1R might affect the binding of **10b** through contact with $H278^{7.43}$. We performed the MD simulations of **10b** in complex with A_1R-$Y271^{7.46}A$ and observed that the ligand loses its hydrogen bonding interactions with $N254^{6.5}$, which might weaken its binding interactions with the orthosteric binding area (Figure S4).

Preliminary Toxicological Analysis of Pyrazolo[3,4-d]-pyridazine Derivatives. Given the high affinity **10b** displays for A_1R and A_3R, and thus the potential for it to be a scaffold for future compound development, we wanted to evaluate its antiproliferative nature as an early indicator of its toxicological profile. We therefore evaluated **10b**, alongside the other compounds in this study, for cytotoxic activity against human fibroblasts (WI-38) and two cancer cell lines, namely the prostate cancer (PC-3) and colon cancer (HCT116) cell lines. Importantly, **10b** alongside all the compounds proved to be not cytotoxic against the cell lines, with IC_{50} values >10 μM. The only compound that did display any cytotoxicity was **15b**, which displayed moderate cytotoxicity against the PC-3 and HCT116 cell lines, showing IC_{50} values of 5.3 ± 0.1 μM against PC-3 cells and 4.15 ± 0.05 μM against HCT116 cells. As a result of these data, we are confident that **10b** is noncytotoxic and can be progressed for further development as a dual A_1R/A_3R antagonist.

■ ASSOCIATED CONTENT

⑤ Supporting Information

The Supporting Information is available free of charge at https://pubs.acs.org/doi/10.1021/acsmedchemlett.2c00052.

Scheme S1. Comparison of amino acid residue sequences of the binding area. Table S1. Chemical structures and antagonistic potencies of 7-amino-pyrazolo[3,4-d]-pyridazines **10a**−**c** and **15a**−**c** against A2AR and A2BR. Table S2. Mean RMSD values for all compounds against A_1R, $A_{2A}R$, and $A_{2B}R$ and ΔG_{eff} only for **10**−**10c** against A_1R. Figure S1. ^1H and ^{13}C NMR spectra of the target compounds. Figure S2. Results from the MD simulations of **10b** and **15b** against A_3R and $A_{2B}R$. Figure S3. Docking poses of 4-(2-phenethyl)amino-1-phenylethyl pyrazolo-[3,4-b]pyridine and N9-methyl,N6-benzyl adenine to A_1R. Figure S4. Representative frames from 100 ns MD simulations of **10b** inside the orthosteric binding area of WT A1R and **10b** inside mutant Y271A A_1R and the receptor−ligand interaction frequency histogram and RMSD graphs of protein Ca and ligand heavy atoms. Information for the methods and synthetic protocols. (PDF)

■ AUTHOR INFORMATION

Corresponding Authors

Antonios Kolocouris − *Laboratory of Medicinal Chemistry, Section of Pharmaceutical Chemistry, Department of Pharmacy, School of Health Sciences, National and Kapodistrian University of Athens, 15771 Athens, Greece;* ⊙ orcid.org/0000-0001-6110-1903; Email: ankol@pharm.uoa.gr

Nikolaos Lougiakis − *Laboratory of Medicinal Chemistry, Section of Pharmaceutical Chemistry, Department of Pharmacy, School of Health Sciences, National and Kapodistrian University of Athens, 15771 Athens, Greece;* Email: nlougiak@pharm.uoa.gr

Graham Ladds − *Department of Pharmacology, University of Cambridge, Cambridge CB2 1PD, U.K.;* ⊙ orcid.org/0000-0001-7320-9612; Email: grl30@cam.ac.ukz

Authors

Anna Suchankova − *Department of Pharmacology, University of Cambridge, Cambridge CB2 1PD, U.K.*

Margarita Stampelou − *Laboratory of Medicinal Chemistry, Section of Pharmaceutical Chemistry, Department of Pharmacy, School of Health Sciences, National and Kapodistrian University of Athens, 15771 Athens, Greece*

Klontiana Koutsouki − *Laboratory of Medicinal Chemistry, Section of Pharmaceutical Chemistry, Department of Pharmacy, School of Health Sciences, National and Kapodistrian University of Athens, 15771 Athens, Greece; Department of Nutrition & Dietetics, School of Health Sciences and Education, Harokopio University, 17671 Athens, Greece;* Present Address: Cyprus Pharmaceutical Organization Limited, 11 King Paul A' Street, 1096 Nicosia, Cyprus

Athanasios Pousias − *Laboratory of Medicinal Chemistry, Section of Pharmaceutical Chemistry, Department of Pharmacy, School of Health Sciences, National and Kapodistrian University of Athens, 15771 Athens, Greece*

Lakshiv Dhingra − *Department of Pharmacology, University of Cambridge, Cambridge CB2 1PD, U.K.*

Kerry Barkan − *Department of Pharmacology, University of Cambridge, Cambridge CB2 1PD, U.K.*

Nicole Pouli − *Laboratory of Medicinal Chemistry, Section of Pharmaceutical Chemistry, Department of Pharmacy, School of Health Sciences, National and Kapodistrian University of Athens, 15771 Athens, Greece*

Panagiotis Marakos − *Laboratory of Medicinal Chemistry, Section of Pharmaceutical Chemistry, Department of Pharmacy, School of Health Sciences, National and Kapodistrian University of Athens, 15771 Athens, Greece*

Roxane Tenta − *Department of Nutrition & Dietetics, School of Health Sciences and Education, Harokopio University, 17671 Athens, Greece*

Complete contact information is available at: https://pubs.acs.org/10.1021/acsmedchemlett.2c00052

Author Contributions

[†]A.S., M.S., and K.K. contributed equally. A.K., N.L. and G.L. contributed equally. A.K., N.L., G.L., and M.S. conceived and designed the research; K.K. and A.P. synthesized and characterized the compounds in the P.M., N.P., and N.L. lab; A.S. and L.D. performed the mammalian assays in the G.L. lab; M.S. performed the simulations in the A.K. lab; K.K., A.P., M.S., A.S., N.L., P.M., A.K., and G.L. analyzed the data; A.K., P.M., N.P., N.L., and G.L. wrote the manuscript; A.K., G.L., N.L., and M.S. edited the manuscript.

Notes

The authors declare no competing financial interest.

■ ABBREVIATIONS

ARs, adenosine receptors; BRET, bioluminescence resonance energy transfer; GPCRs, G protein-coupled receptors; HEK, human embryonic kidney; MD, molecular dynamics; NECA, 5′-N-ethylcarboxamidoadenosine; PDB, Protein Data Bank; RMSD, root-mean-square deviation; T_c, TanimotoCombo; t_m, mixing time; TM, transmembrane

■ REFERENCES

(1) Fredholm, B. B.; IJzerman, A. P.; Jacobson, K. A.; Linden, J.; Muller, C. E.; Müller, C. E. International Union of Basic and Clinical Pharmacology. LXXXI. Nomenclature and Classification of Adenosine Receptors — An Update. *Pharmacol. Rev.* **2011**, *63*, 1−34.

(2) Schenone, S.; Brullo, C.; Musumeci, F.; Bruno, O.; Botta, M. A1 Receptors Ligands: Past, Present and Future Trends. *Curr. Top. Med. Chem.* **2010**, *10*, 878−901.

(3) Squarcialupi, L.; Catarzi, D.; Varano, F.; Betti, M.; Falsini, M.; Vincenzi, F.; Ravani, A.; Ciancetta, A.; Varani, K.; Moro, S.; Colotta, V. Structural Refinement of Pyrazolo[4,3-d]Pyrimidine Derivatives to Obtain Highly Potent and Selective Antagonists for the Human A3 Adenosine Receptor. *Eur. J. Med. Chem.* **2016**, *108*, 117−133.

(4) Sun, B.; Bachhawat, P.; Chu, M. L.-H.; Wood, M.; Ceska, T.; Sands, Z. A.; Mercier, J.; Lebon, F.; Kobilka, T. S.; Kobilka, B. K. Crystal Structure of the Adenosine A2A Receptor Bound to an Antagonist Reveals a Potential Allosteric Pocket. *Proc. Natl. Acad. Sci. U. S. A.* **2017**, *114*, 2066−2071.

(5) el-Hashim, A.; D'Agostino, B.; Matera, M. G.; Page, C. Characterization of adenosine receptors involved in adenosine-induced bronchoconstriction in allergic rabbits. *Br. J. Pharmacol.* **1996**, *119*, 1262−1268.

(6) Brown, R. A.; Spina, D.; Page, C. P. Adenosine receptors and asthma. *Br. J. Pharmacol.* **2008**, *153*, S446−S456.

(7) Johnson, J. A.; Montgomery, A. P.; Starr, E. R.; Ludwig, J.; Trevitt, J. Dose-dependent effects of adenosine antagonists on tacrine-induced tremulous jaw movements. *Eur. J. Pharmacol.* **2018**, *833*, 364−369.

(8) Cohen, S.; Fishman, P. Targeting the A3 Adenosine Receptor to Treat Cytokine Release Syndrome in Cancer Immunotherapy. *Drug Des. Devel. Ther.* **2019**, *13*, 491−497.

(9) Lee, J.; Hwang, I.; Lee, J. H.; Lee, H. W.; Jeong, L.-S.; Ha, H. The Selective A3AR Antagonist LJ-1888 Ameliorates UUO-Induced Tubulointerstitial Fibrosis. *Am. J. Pathol.* **2013**, *183*, 1488−1497.

(10) Wang, Z.; Do, C. W.; Avila, M. Y.; Peterson-Yantorno, K.; Stone, R. A.; Gao, Z.-G.; Joshi, B.; Besada, P.; Jeong, L. S.; Jacobson, K. A.; Civan, M. M. Nucleoside-Derived Antagonists to A3 Adenosine Receptors Lower Mouse Intraocular Pressure and Act across Species. *Exp. Eye Res.* **2010**, *90*, 146−154.

(11) Glukhova, A.; Thal, D. M.; Nguyen, A. T.; Vecchio, E. A.; Jörg, M.; Scammells, P. J.; May, L. T.; Sexton, P. M.; Christopoulos, A. Structure of the Adenosine A1 Receptor Reveals the Basis for Subtype Selectivity. *Cell* **2017**, *168*, 867−877.

(12) Cheng, R. K. Y.; Segala, E.; Robertson, N.; Deflorian, F.; Doré, A. S.; Errey, J. C.; Fiez-Vandal, C.; Marshall, F. H.; Cooke, R. M. Structures of Human A1 and A2A Adenosine Receptors with Xanthines Reveal Determinants of Selectivity. *Structure* **2017**, *25*, 1275−1285.

(13) Draper-Joyce, C. J.; Khoshouei, M.; Thal, D. M.; Liang, Y.-L.; Nguyen, A. T. N.; Furness, S. G. B.; Venugopal, H.; Baltos, J.-A.; Plitzko, J. M.; Danev, R.; Baumeister, W.; May, L. T.; Wootten, D.; Sexton, P.

M.; Glukhova, A.; Christopoulos, A. Structure of the Adenosine-Bound Human Adenosine A1 Receptor-Gi Complex. *Nature* **2018**, *558*, 559−563.

(14) Stampelou, M.; Suchankova, A.; Tzortzini, E.; Dhingra, L.; Barkan, K.; Lougiakis, N.; Marakos, P.; Pouli, N.; Ladds, G.; Kolocouris, A. Novel Pyrazolo[3,4-c]Pyridine Antagonists with Nanomolar Affinity for A1/A3 Adenosine Receptors: Binding Kinetics and Exploration of Their Binding Profile Using Mutagenesis Experiments, MD Simulations and TI/MD Calculations. *ChemRxiv* **2021**, DOI: 10.26434/chemrxiv-2021-j18mg-v3.

(15) Catarzi, D.; Colotta, V.; Varano, F.; Poli, D.; Squarcialupi, L.; Filacchioni, G.; Varani, K.; Vincenzi, F.; Borea, P. A.; Dal Ben, D.; Lambertucci, C.; Cristalli, G. Pyrazolo[1,5-c]Quinazoline Derivatives and Their Simplified Analogues as Adenosine Receptor Antagonists: Synthesis, Structure-Affinity Relationships and Molecular Modeling Studies. *Bioorg. Med. Chem.* **2013**, *21*, 283−294.

(16) Manetti, F.; Schenone, S.; Bondavalli, F.; Brullo, C.; Bruno, O.; Ranise, A.; Mosti, L.; Menozzi, G.; Fossa, P.; Trincavelli, M. L.; Martini, C.; Martinelli, A.; Tintori, C.; Botta, M. Synthesis and 3D QSAR of new pyrazolo[3,4-b]pyridines: potent and selective inhibitors of A1 adenosine receptors. *J. Med. Chem.* **2005**, *48*, 7172−7185.

(17) Tuccinardi, T.; Zizzari, A. T.; Brullo, C.; Daniele, S.; Musumeci, F.; Schenone, S.; Trincavelli, M. L.; Martini, C.; Martinelli, A.; Giorgi, G.; Botta, M. Substituted pyrazolo[3,4-b]pyridines as human A1 adenosine antagonists: Developments in understanding the receptor stereoselectivity. *Org. Biomol. Chem.* **2011**, *9*, 4448−4455.

(18) Cheong, S. L.; Venkatesan, G.; Paira, P.; Jothibasu, R.; Mandel, A. L.; Federico, S.; Spalluto, G.; Pastorin, G. Pyrazolo Derivatives as Potent Adenosine Receptor Antagonists: An Overview on the Structure-Activity Relationships. *Int. J. Med. Chem.* **2011**, 480652.

(19) Barkan, K.; Lagarias, P.; Stampelou, M.; Stamatis, D.; Hoare, S.; Safitri, D.; Klotz, K.-N.; Vrontaki, E.; Kolocouris, A.; Ladds, G. Pharmacological Characterisation of Novel Adenosine A3 Receptor Antagonists. *Sci. Rep.* **2020**, *10*, 20781.

(20) Lagarias, P.; Barkan, K.; Tzortzini, E.; Stampelou, M.; Vrontaki, E.; Ladds, G.; Kolocouris, A. Insights to the Binding of a Selective Adenosine A3 Receptor Antagonist Using Molecular Dynamic Simulations, MM-PBSA and MM-GBSA Free Energy Calculations, and Mutagenesis. *J. Chem. Inf. Model.* **2019**, *59*, 5183−5197.

(21) Papastathopoulos, A.; Lougiakis, N.; Kostakis, I. K.; Marakos, P.; Pouli, N.; Pratsinis, H.; Kletsas, D. New Bioactive 5-Arylcarboximidamidopyrazolo[3,4-c]Pyridines: Synthesis, Cytotoxic Activity, Mechanistic Investigation and Structure-Activity Relationships. *Eur. J. Med. Chem.* **2021**, *218*, 113387.

(22) Bento, A. P.; Gaulton, A.; Hersey, A.; Bellis, L. J.; Chambers, J.; Davies, M.; Krüger, F. A.; Light, Y.; Mak, L.; McGlinchey, S.; Nowotka, M.; Papadatos, G.; Santos, R.; Overington, J. P. The ChEMBL Bioactivity Database: An Update. *Nucleic Acids Res.* **2014**, *42*, D1083−D1090.

(23) Hawkins, P. C. D.; Skillman, A. G.; Nicholls, A. Comparison of Shape-Matching and Docking as Virtual Screening Tools. *J. Med. Chem.* **2007**, *50*, 74−82.

(24) Pei, Y.; Wickham, B. O. S. Regioselective Syntheses of 3-Aminomethyl-5-Substituted Isoxazoles: A Facile and Chemoselective Reduction of Azide to Amine by Sodium Borohydride Using 1,3-Propanedithiol as a Catalyst. *Tetrahedron Lett.* **1993**, *34*, 7509−7512.

(25) Fadnavis, N. W.; Radhika, K. R. Enantio- and Regiospecific Reduction of Ethyl 4-Phenyl-2,4-Dioxobutyrate with Baker's Yeast: Preparation of (R)-HPB Ester. *Tetrahedron Asymmetry* **2004**, *15*, 3443−3447.

(26) Dang, T. T.; Dang, T. T.; Fischer, C.; Görls, H.; Langer, P. Synthesis of Pyrazole-3-Carboxylates and Pyrazole-1,5-Dicarboxylates by One-Pot Cyclization of Hydrazone Dianions with Diethyl Oxalate. *Tetrahedron* **2008**, *64*, 2207−2215.

(27) Yan, Z.; Liu, A.; Huang, M.; Liu, M.; Pei, H.; Huang, L.; Yi, H.; Liu, W.; Hu, A. Design, Synthesis, DFT Study and Antifungal Activity of the Derivatives of Pyrazolecarboxamide Containing Thiazole or Oxazole Ring. *Eur. J. Med. Chem.* **2018**, *149*, 170−181.

(28) Schmidt, A.; Habeck, T.; Kindermann, M. K.; Nieger, M. New Pyrazolium-Carboxylates as Structural Analogues of the Pseudo-Cross-Conjugated Betainic Alkaloid Nigellicine. *J. Org. Chem.* **2003**, *68*, 5977−5982.

(29) Knight, A.; Hemmings, J. L.; Winfield, I.; Leuenberger, M.; Frattini, E.; Frenguelli, B. G.; Dowell, S. J.; Lochner, M.; Ladds, G. Discovery of Novel Adenosine Receptor Agonists That Exhibit Subtype Selectivity. *J. Med. Chem.* **2016**, *59*, 947−964.

(30) Stoddart, L. A.; Vernall, A. J.; Denman, J. L.; Briddon, S. J.; Kellam, B.; Hill, S. J. Fragment Screening at Adenosine-A3 Receptors in Living Cells Using a Fluorescence-Based Binding Assay. *Chem. Biol.* **2012**, *19*, 1105−1115.

(31) Eldridge, M. D.; Murray, C. W.; Auton, T. R.; Paolini, G. V.; Mee, R. P. Empirical Scoring Functions: I. The Development of a Fast Empirical Scoring Function to Estimate the Binding Affinity of Ligands in Receptor Complexes. *J. Comput. Aided. Mol. Des.* **1997**, *11*, 425−445.

(32) Hornak, V.; Abel, R.; Okur, A.; Strockbine, B.; Roitberg, A.; Simmerling, C. Comparison of Multiple Amber Force Fields and Development of Improved Protein Backbone Parameters. *Proteins Struct. Funct. Genet.* **2006**, *65*, 712−725.

(33) Massova, I.; Kollman, P. A. Combined molecular mechanical and continuum solvent approach (MM-PBSA/GBSA) to predict ligand binding. *Per. Drug Discovery Design* **2000**, *18*, 113−135.

(34) Wang, E.; Sun, H.; Wang, J.; Wang, Z.; Liu, H.; Zhang, J. Z. H.; Hou, T. End-Point Binding Free Energy Calculation with MM/PBSA and MM/GBSA: Strategies and Applications in Drug Design. *Chem. Rev.* **2019**, *119*, 9478−9508.

(35) Kaminski, G.; Friesner, R. A.; Tirado-Rives, J.; Jorgensen, W. L. Evaluation and Reparametrization of the OPLS-AA Force Field for Proteins via Comparison with Accurate Quantum Chemical Calculations on Peptides. *Phys. Chem. B* **2001**, *105* (28), 6474−6487.

(36) Shivakumar, D.; Williams, J.; Wu, Y.; Damm, W.; Shelley, J.; Sherman, W. Prediction of Absolute Solvation Free Energies using Molecular Dynamics Free Energy Perturbation and the OPLS Force Field. *J. Chem. Theory Comput.* **2010**, *6*, 1509−19.

(37) Stamatis, D.; Lagarias, P.; Barkan, K.; Vrontaki, E.; Ladds, G.; Kolocouris, A. Structural Characterization of Agonist Binding to an A3 Adenosine Receptor through Biomolecular Simulations and Mutagenesis Experiments. *J. Med. Chem.* **2019**, *62*, 8831−8846.